NMR Studies of the Anti-Apoptotic Protein Bcl-x_L in Micelles

Judit A. Losonczi, Edward T. Olejniczak, Stephen F. Betz, John E. Harlan, Jamey Mack, and Stephen W. Fesik*

Pharmaceutical Discovery Division, Abbott Laboratories, Abbott Park, IL 60064

Received April 24, 2000; Revised Manuscript Received June 23, 2000

ABSTRACT: The Bcl-2 family of proteins play a pivotal role in the regulation of programmed cell death. One of the postulated mechanisms for the function of these proteins involves the formation of ion channels in membranes. As a first step to structurally characterize these proteins in a membrane environment, we investigated the structure of a Bcl-x_L mutant protein when incorporated into small detergent micelles. This form of Bcl-x_L lacks the loop (residues 49−88) between helix 1 and helix 2 and the putative C-terminal transmembrane helix (residues 214−237). Below the critical micelle concentration (CMC), Bcl-x_L binds detergents in the hydrophobic groove that binds to pro-apoptotic proteins. However, above the CMC, Bcl-x_L undergoes a dramatic conformational change. Using NMR methods, we characterized the secondary structure of Bcl-x_L in the micelle-bound form. Like Bcl-x_L in aqueous solution, the structure of the protein when dissolved in dodecylphosphocholine (DPC) micelles consists of several α-helices separated by loops. However, the length and position of the individual helices of Bcl-x_L in micelles differ from those in aqueous solution. The location of Bcl-x_L within the micelle was examined from the analysis of protein−detergent NOEs and limited proteolysis. In addition, the mobility of the micelle-bound form of Bcl-x_L was investigated from NMR relaxation measurements. On the basis of these studies, a model is proposed for the structure, dynamics, and location of Bcl-x_L in micelles. In this model, Bcl-x_L has a loosely packed, dynamic structure in micelles, with helices 1 and 6 and possibly helix 5 partially buried in the hydrophobic interior of the micelle. Other parts of the protein are located near the surface or on the outside of the micelle.

The Bcl-2 family of proteins regulate apoptosis, an essential physiological mechanism for the selective elimination of cells.[1] Dysregulation of programmed cell death can contribute to a variety of diseases, including cancer, autoimmunity, and neurodegenerative disorders (*1*). Members of the Bcl-2 family can be divided into two main categories: anti-apoptotic proteins such as Bcl-2, Bcl-x_L, and Bcl-w, which inhibit programmed cell death and proteins that promote cell death such as Bak, Bax, or Bad (*2*). The structure of an anti-apoptotic family member, Bcl-x_L, has been determined (*3*). It consists of two central, primarily hydrophobic α-helices (helix 5 and helix 6), which are surrounded by five amphipathic helices. A long loop connecting helix 1 and helix 2 was found to be flexible and nonessential for anti-apoptotic activity (*3*). A key feature of the structure was the presence of an elongated hydrophobic cleft, which was later shown to mediate heterodimerization of pro- and anti-apoptotic family members by binding of an amphipathic α-helix of pro-apoptotic proteins (*4*).

The structure of Bcl-x_L is reminiscent of the pore-forming domain of bacterial toxins that function by forming ion channels in biological membranes (*3*). On the basis of this structural similarity, we postulated that Bcl-x_L may also form channels, which was subsequently demonstrated using synthetic lipid membranes (*5*). It has also been shown that Bcl-2 (*6*), Bax (*7*, *8*), and Bid (*9*) all share this channel-forming ability. Like the bacterial pore-forming proteins, the ion channels formed by Bcl-2 proteins exhibit multiple conductance states, and channel formation is favored by changes in membrane potential or pH. In general, Bcl-x_L and Bcl-2 form channels that have low conductance, display moderate cation selectivity, and mostly exist in a closed state; whereas, Bax channels typically exhibit a 100−1000-fold larger conductance than Bcl-x_L or Bcl-2 channels, prefer anions, and exist for a longer time in the open state (*10*). By analogy to the structurally similar pore-forming domains of bacterial toxins, helix 5 and helix 6 of Bcl-x_L and Bcl-2 are hypothesized to directly participate in channel formation. Indeed, deletion of parts of helix 5 and helix 6 from Bcl-2 abolishes its ability to form ion channels in vitro (*6*). These results suggest that the capability to form ion channels is critical for the biological functions of the Bcl-2 family of proteins. Such pore formation has been hypothesized to be important for regulating the release of cytochrome *c* or perturbing mithochondrial physiology (*11*).

An understanding of the structure of the Bcl-2 family of proteins in their membrane-associated form could help to answer some of the many questions on their mode of action in the regulation of apoptosis. However, structural studies of membrane proteins in lipids or lipid-like systems is

* To whom correspondence should be addressed. Dr. Stephen W. Fesik, Abbott Laboratories, D-47G, AP10-LL, 100 Abbott Park Road, Abbott Park, IL 60064. Phone: (847) 937-1201; fax: (847) 938-2478; e-mail: stephen.fesik@abbott.com.

[1] Abbreviations: CD, circular dichroism; CMC, critical micelle concentration; DHPC, 1,2-dihexanoyl-phosphatidylcholine; DPC, dodecylphosphocholine; HSQC, heteronuclear single quantum coherence; LPC, lyso-1-myristoyl-phosphatidylcholine; NMR, nuclear magnetic resonance; NOESY, nuclear Overhauser-effect spectroscopy; SDS, sodium dodecyl sulfate; TOCSY, total correlation spectroscopy.

10.1021/bi000919v CCC: $19.00
Published on Web 08/17/2000

technically challenging. One possible approach for studying membrane proteins by NMR involves the use of detergent micelles as a mimic of a membrane-like environment. The advantage of using micelles is that peptides and proteins incorporated in micelles still tumble fast enough to enable the use of high-resolution NMR. Indeed, in recent years, the structures of many small proteins have been studied in detergent micelles using NMR spectroscopy (*12*−*15*).

As a first step to characterize the membrane-bound form of Bcl-x_L, we have studied Bcl-x_L in micelles. This was accomplished using a combination of high-resolution NMR techniques, CD spectroscopy, limited proteolytic digestion, and analytical ultracentrifugation.

MATERIALS AND METHODS

Protein Expression and Purification. The deletion mutant of Bcl-x_L used in these studies lacks the putative C-terminal transmembrane region (FNRWFLTGMTVAGVVLLGSLF-SRK) and residues 49−88, which constitute a flexible loop previously shown to be dispensable for the anti-apoptotic activity of the protein (*3*). In this paper, we refer to the above deletion mutant as Bcl-x_L. Residue numbers in the text correspond to those of full-length Bcl-x_L.

Uniformly ^{15}N- or ^{15}N-^{13}C-labeled protein was obtained by growing the *Escherichia coli* strain HMS174(DE3) on M9 medium containing $^{15}NH_4Cl$ with unlabeled or [U-^{13}C]-glucose accordingly. Fractionally or perdeuterated, ^{15}N,-^{13}C-labeled protein was prepared by growing cells in 75 or 100% D_2O, respectively. Recombinant Bcl-x_L was purified by affinity chromatography on a nickel-IDA column (Invitrogen). Further purification was achieved by reverse-phase chromatography of the denatured protein on a C4 or C8 column, followed by refolding through the gradual removal of the denaturant by dialysis. Selective ^{15}N labeling was accomplished by growing the cells in M9 media supplemented with selected ^{15}N-labeled amino acids.

Sample Preparation. Bcl-x_L-containing micelles were prepared by mixing a solution of the water-soluble protein and a detergent-containing solution. The detergents used in the studies were dodecylphosphocholine (DPC), 1,2-dihexanoyl-phosphatidylcholine (DHPC), lyso-1-myristoyl-phosphatidylcholine (LPC), and sodium dodecyl sulfate (SDS).

Circular Dichroism (CD). CD measurements were obtained using a Jasco J-715 spectropolarimeter at 25 °C in a quartz cell of 0.01-cm path length. The spectra were collected using a protein concentration of 50 μM in a phosphate buffer (pH 7) with 2, 5, and 50 mM detergent (DPC, SDS, or DHPC). A baseline of pure detergent solution was recorded and subtracted from each spectrum.

Analytical Ultracentrifugation. Sedimentation equilibrium experiments were performed at 25 °C on Bcl-x_L in DPC micelles using a Beckman XL-I analytical ultracentrifuge. Studies were carried out in 20 mM HEPES (pH 7.4), 100 mM NaCl, and 50 mM DPC. Following the method of Reynolds and Tanford (*16, 17*) as implemented by Kochendoerfer for DPC (*18*), the density of the buffer was adjusted to that of the detergent by the addition of 52.5% D_2O. In this way, the contribution to the molecular buoyancy from the detergent in a protein−detergent aggregate is negligible, and the molecular weight reflects only the protein. Samples were centrifuged in three compartment carbon-epoxy centerpieces filled with 130 μL of fluid for each channel (sample and blank) at three protein concentrations. Measurements were obtained using buffer and buffer plus 50 mM DPC as blanks. Equilibrium absorbance measurements at 280 nm were obtained at three rotor speeds (10 200, 21 000, and 30 000 rpm). These were analyzed globally by a nonlinear least squares curve fitting of radial concentration profiles using the Marquardt−Levenberg algorithm as implemented in Origin 5.0 (Microcal Software, Inc., Northampton, MA). A user defined function describing sedimentation behavior of discrete particles was used (see eq 1 in ref *19*). Baselines and fixed radius signal values for each data set were allowed to vary independently; however, the molecular weight was held as a global parameter. The partial specific volume of the protein was calculated from the amino acid composition by the method of Cohn and Edsall as 0.705 cm^3/g (*20*). Buffer density was measured as 1.06175 g/cm^3 in a Mettler-KEM Da-310 density meter.

Partial Proteolysis. Limited proteolytic digestion was performed using 0.15 mM (3 mg/mL) Bcl-x_L in 40 mM phosphate buffer (pH 7.0), with and without 40 mM DPC. The samples were incubated at 25 °C for 1 h with 0.06 mg/mL trypsin, 0.06 mg/mL chymotrypsin, or 0.03 mg/mL endoproteinase Glu-C. The reactions were stopped with PMSF. The digests were analyzed using LC-MS by injecting 5-μL samples onto a C4 reverse phase HPLC column followed by electrospray MS using a Micromass Q-TOF mass spectrometer. The data were analyzed using the programs MassLynx (Micromass) and PAWS (Proteometrics).

NMR Spectroscopy. NMR samples contained 1−2 mM Bcl-x_L in 200 mM DPC-d_{38}, 40 mM sodium phosphate (pH 7.0), 5 mM perdeuterated DTT, and H_2O/D_2O 9:1 (except where noted). NMR spectra were acquired at 37 °C on Bruker DRX500, DRX600, and DRX800 MHz NMR spectrometers. All instruments were equipped with z- or xyz-shielded gradient triple resonance probes. The experiments employed in the present study were 2D [^{15}N, ^1H]-HSQC (*21*), 2D ct-[^{13}C, ^1H]-HSQC in D_2O (*22*), 3D HNCO (*23*), 3D HN-(CA)CO (*24*), 3D HNCA (*25*), 3D HN(CO)CA, 3D HNCACB, 3D HN(COCA)CB (*26*), 3D HA(CACO)NH, 3D HACACO in D_2O (*27*), 3D HCCH-TOCSY in D_2O (*28*), 3D (H)-C-(C-CO)HN TOCSY, 3D H-(CC-CO)HN TOCSY (*29*), ^{15}N-resolved [^1H, ^1H] TOCSY (*30*), 3D ^{15}N-resolved [^1H, ^1H] NOESY (*31*), 3D ^{13}C-resolved [^1H, ^1H] NOESY in D_2O (*32*), and 3D HNHA (*33*). For the backbone experiments, a 100% perdeuterated ^{15}N, ^{13}C sample was used, while for side chain assignments a protonated ^{15}N, ^{13}C sample was employed. The 3D (H)-C-(C-CO)HN TOCSY and 3D H-(CC-CO)HN TOCSY experiments were recorded on a 70% deuterated ^{15}N, ^{13}C sample. To identify detergent−protein NOEs, a 3D ^{15}N-resolved [^1H, ^1H] NOESY was also performed using a mixing time of 200 ms on a 100% perdeuterated ^{15}N, ^{13}C sample in fully protonated DPC. This sample allowed the observation of NN(i,i+1) NOEs that could be used to aid in the HN assignments.

NMR experiments involving amide proton detection employed pulsed field gradients for coherence pathway transfer selection (*34*−*36*), using the enhanced sensitivity approach (*37*). Saturation of water was minimized through the use of "water selective flip back pulses" and gradients and by ensuring that water magnetization is placed along the +z axis immediately prior to acquisition (*38*). For

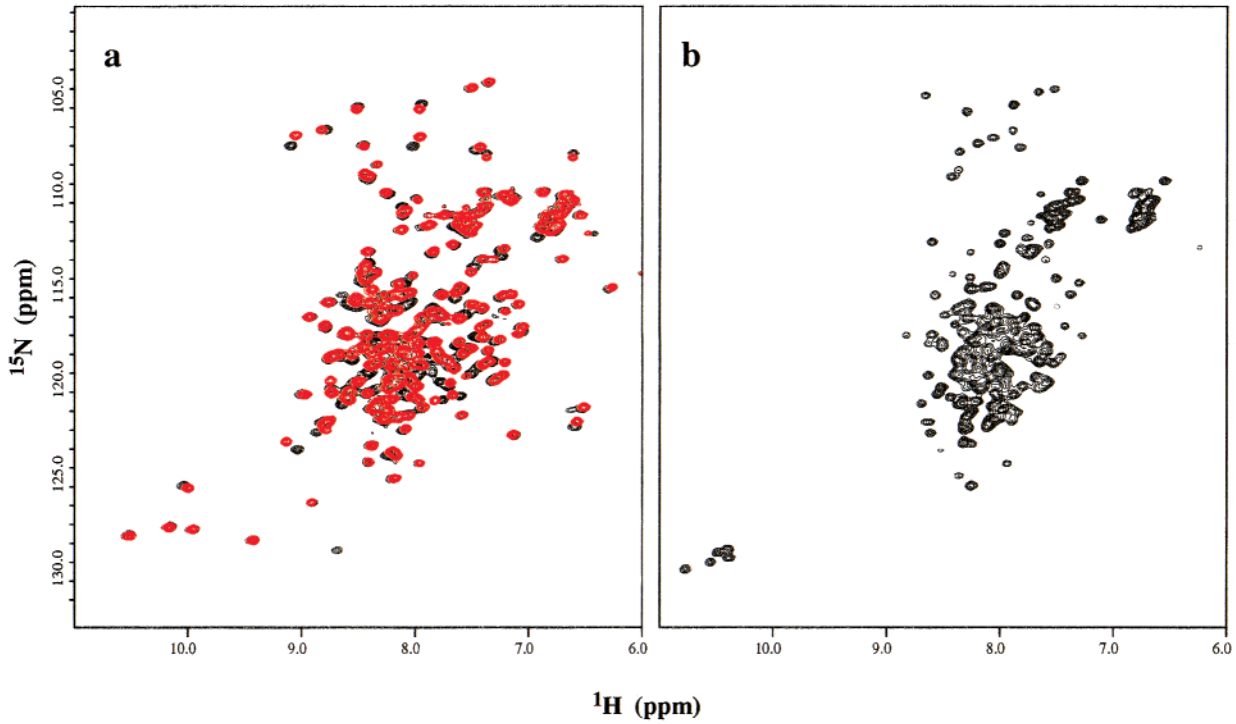

FIGURE 1: Comparison of the 2D [^{15}N,^{1}H]-HSQC spectrum of Bcl-x_L in a detergent-free and in a DPC micelle environment. (a) Overlay of the HSQC spectrum of Bcl-x_L in water (black) and in 0.5 mM DPC (red). (b) HSQC spectrum of Bcl-x_L in 100 mM DPC (above the CMC, which is 1 mM). The protein concentration is 1 mM in 40 mM phosphate buffer (pH 7).

experiments on the samples in D_2O, a presaturation pulse was used for water suppression.

Typical carrier positions employed in the double- and triple-resonance experiments were 115.6 ppm for ^{15}N, 175 ppm for ^{13}CO, 55 ppm for $^{13}C_\alpha$, 42 ppm for $^{13}C_\beta$, 4.7 ppm for ^{2}H, and 4.68 ppm for ^{1}H. For the ^{13}C-resolved [^{1}H,^{1}H] NOESY and the ^{13}C/^{13}C-resolved [^{1}H,^{1}H] NOESY experiments, the carrier was placed at 72 ppm with a ^{13}C sweep width of 43 ppm, resulting in folding of the aromatic and part of the aliphatic signals. ^{15}N, ^{2}H, and ^{1}H decoupling was accomplished using WALTZ-16 (*39*), while GARP (*40*) was used for ^{13}C decoupling. Where necessary (e.g., in the HNCACB experiment), carbonyl decoupling from C_α was achieved by the use of a soft G3 pulse (*41*) at 175 ppm. The DIPSY-2 (*42*) mixing scheme was employed in the TOCSY-type experiments.

Quadrature detection in all of the indirectly detected dimensions was achieved via States-TPPI (*30*). The data were processed and analyzed using in-house written software on Silicon Graphics computers. Typical data processing involved linear prediction in the indirect dimensions and zero filling to twice the collected data size in all dimensions (*43*).

^{15}N Backbone Relaxation. A series of inverse detected 2D [^{1}H,^{15}N] NMR experiments were employed to characterize the ^{15}N T_1 and T_2 relaxation times and heteronuclear [^{1}H,^{15}N] steady-state NOE values of Bcl-x_L in micelles at 600 MHz (*44*). The *T*1 experiment was recorded with seven delays of 11, 55, 110, 165, 270, 490, and 820 ms, and the delays used in the *T*2 experiments were 15, 29, 43, 57, 72, 100, and 145 ms. ^{1}H-^{15}N NOE values were determined from two spectra recorded with and without ^{1}H saturation.

Amide Exchange Rates. Amide exchange rates were initially studied by using a series of 800-MHz [^{15}N,^{1}H]-HSQC spectra after a 10-fold dilution of a 2 mM Bcl-x_L/100 mM DPC-d_{38} sample with DPC containing D_2O buffer. Exchange data were quantified by measuring HN-H_2O cross-peak intensities in the 100-ms 3D ^{15}N-resolved [^{1}H,^{1}H] NOESY experiment.

RESULTS AND DISCUSSION

Binding of Detergents to Bcl-x_L. To test for changes that might occur to Bcl-x_L upon the addition of detergents, we titrated a variety of commonly used detergents (DPC, DHPC, LPC, and SDS) into an aqueous solution of uniformly ^{15}N-labeled Bcl-x_L. Changes in the structure and chemical environment of Bcl-x_L were identified from the shifts observed in a 2D [^{15}N,^{1}H]-HSQC spectrum. Figure 1 illustrates the effect of adding DPC on the HSQC spectrum of Bcl-x_L. The addition of DPC below its critical micelle concentration (CMC) results in specific chemical shift changes (Figure 1a). The same chemical shift changes were observed for all of the tested detergents, indicating a specific and common interaction between Bcl-x_L and the detergents. The chemical shift changes occur for residues in or near the hydrophobic cleft of Bcl-x_L (e.g., Gly98, Val126, Gly129, Phe150, Gly151, Gly152, and Arg169) that is responsible for binding to pro-apoptotic Bcl-2 family members (*4*).

With increasing detergent concentration, the protein undergoes an abrupt conformational change that is indicated by the appearance of a new set of resonances as illustrated in Figure 1b. This change occurs at 3−10 times the CMC of the detergents. These results clearly show that Bcl-x_L undergoes a major conformational change that only occurs upon interaction with micelles. The presence of monomeric, water-soluble detergent below its CMC does not trigger this conformational change as evidenced by the lack of large changes in the amide chemical shifts for residues throughout

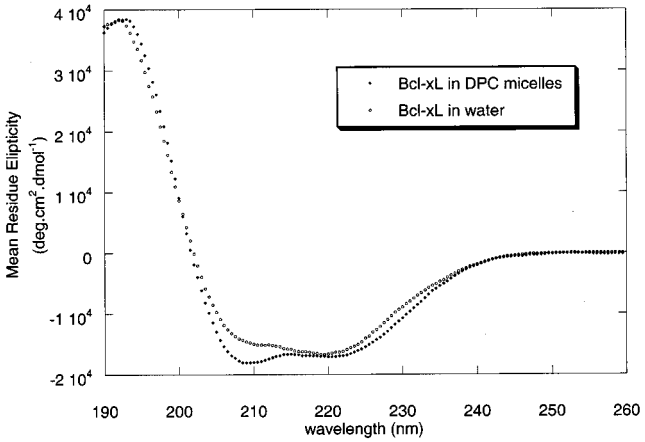

FIGURE 2: Comparison of the circular dichroism (CD) spectrum of Bcl-x_L in water and in a DPC micelle environment. The estimated helical content is 47% for the micelle bound form and only 34% for the water-dissolved form of Bcl-x_L.

the protein. Similar observations have been made in the case of the apolipoprotein apolipophorin III (*45*).

CD Studies. The chemical shift dispersion of Bcl-x_L in the detergent-solubilized form is much less than that observed for Bcl-x_L in water. To determine whether this change is due to the conversion of Bcl-x_L to an unfolded state, the CD spectrum of the micelle-bound form of Bcl-x_L was recorded (Figure 2). The CD spectrum shows that the protein in micelles has significant α-helical content as indicated by the strong positive band at 190 nm and the broad minima between 205 and 222 nm (*46*). In fact, the overall helicity of the protein is slightly increased upon its interaction with micelles.

Resonance Assignments. The sequence specific backbone resonance assignments of Bcl-x_L in micelles were made using a series of deuterium-decoupled triple-resonance experiments [HNCA, HN(CO)CA, HNCA, HN(CO)CA, HNCACB, and HN(COCA)CB] (*47*−*49*). The use of all six backbone experiments was necessary to resolve the overlap resulting from the very limited chemical shift dispersion of the protein in DPC micelles. From these experiments, more than 90% of the backbone resonances could be assigned. The signals corresponding to Ala96−Glu100 and Ala153−Asp160 were not detected in any of the triple resonance NMR experiments, which is likely due to slow conformational exchange that broadens their NMR signals. However, most of these residues could be identified based on the ^{15}N-resolved NOESY and by the use of 2D-[^{15}N,^{1}H]-HSQC spectra of Bcl-x_L selectively ^{15}N-labeled with Val, Leu, or Lys. The only residues that could not be assigned include the three N-terminal residues, Ala97, Leu154, and Glu157−Val159. Surprisingly, residues in the long, unstructured flexible loop of Bcl-x_L (residues 26−45) exhibit better amide (^{15}N and ^{1}H) chemical shift resolution than other residues in the protein.

The side chain ^{1}H and ^{13}C resonances were assigned by correlating these signals to the backbone amide ^{15}N and HN frequencies that exhibited the highest spectral dispersion. This was accomplished using H-(CC-CO)NH TOCSY and (H)-C(C-CO)NH TOCSY experiments (*50*). An HCCH-TOCSY and an ^{15}N-resolved [^{1}H, ^{1}H] TOCSY experiment were also acquired to aid in assigning the side chain resonances (*48*, *49*). To obtain H_α assignments, HA(CACO)NH and HACACO experiments were employed.

Secondary and Tertiary Structure of Bcl-x_L in Micelles. Deviations from random coil chemical shifts offer insight into the conformation of a protein. For example, H_α resonances experience an upfield shift when located in an α-helix and a downfield shift when present in a β-sheet (*51*). In addition C_α and C′ resonances are shifted downfield when present in an α-helix and shifted upfield when located in a β-sheet (*52*). The program TALOS (*53*) was used to predict the local conformation of Bcl-x_L in micelles from the chemical shifts of the backbone atoms (Figure 3).

Another parameter often used to aid the identification of secondary structure is the amide exchange rate, since slow exchange rates are indicative of amides that are involved in hydrogen bonds. Amide exchange rates can also be used to identify segments of the protein that are buried in the hydrophobic core of the micelle (*54*), although the highly dynamic nature of micelle systems often makes such interpretation difficult. For example, in the case of the Ike major coat protein only very slight differences were observed between the amide exchange rate of residues in the transmembrane and surface associated helices (*13*). On the other hand, in the case of subunit c of the ATP synthase, most residues exchanged within an hour, but some were observable for several days (*15*). In the micelle environment, most of the amides of Bcl-x_L are exchanged in less than an hour. Because of the extensive resonance overlap, it was only possible to unambiguously identify certain well resolved protected amides such as Leu17 in helix 1 and Ala171 and Met174 in helix 6 that did not fully exchange in an hour. The amide exchange rates, although rapid, could still be placed into three categories based on the intensity of an exchange cross-peak with water in the ^{15}N-resolved NOESY spectra (Figure 3). Amides that have exchange rates that are much slower than the experimental mixing time do not show exchange cross-peaks to water in the spectra, while amides with exchange rates that are similar to the experimental mixing time of 100 ms have very intense exchange cross-peaks.

The most important information used in determining the secondary structure of a protein by NMR are the characteristic short-range NOEs (*55*). Helical secondary structure is characterized by sequential NN(i,i+1) and short-range αN(i,i+3) NOEs. The survey of sequential and short-range NOEs is presented in Figure 3 along with the secondary structural elements derived for the protein in DPC micelles. The chemical shift data, the amide exchange rates, and the $^3J_{N\alpha}$ vicinal coupling constants (*56*) are all consistent with the NOE-derived secondary structure.

As shown in Figures 3 and 4, Bcl-x_L in micelles contains seven α-helices. Helix 1 consists of 14 amino acids and is followed by a long, unstructured loop. Helix 2 is very short (only five residues), while helices 3, 4, and 5 are all 10−15 residues in length. The unstructured regions between helices 3 and 4 and helices 5 and 6 are surprisingly long (over 10 amino acids). Helix 6 is the longest of the α-helices and extends from Glu163 to Gln187. A kink is located at the C-terminal end of this helix at Pro184.

In an attempt to characterize the overall fold of the protein in micelles, several medium- and long-range NOE constraints were identified. In particular the following NOEs were observed: Leu21(H_δ)−Tyr26(H_α), Thr113(H_α,H_β)−Ile118(H_β,H_δ), Leu134(H_δ)−Val139(H_α,H_γ), Phe135(H_ϵ,H_δ)−Ile144(H_δ), Val139(H_γ)−Ile144(H_δ,H_γ), Tyr177(H_δ,H_ϵ)−

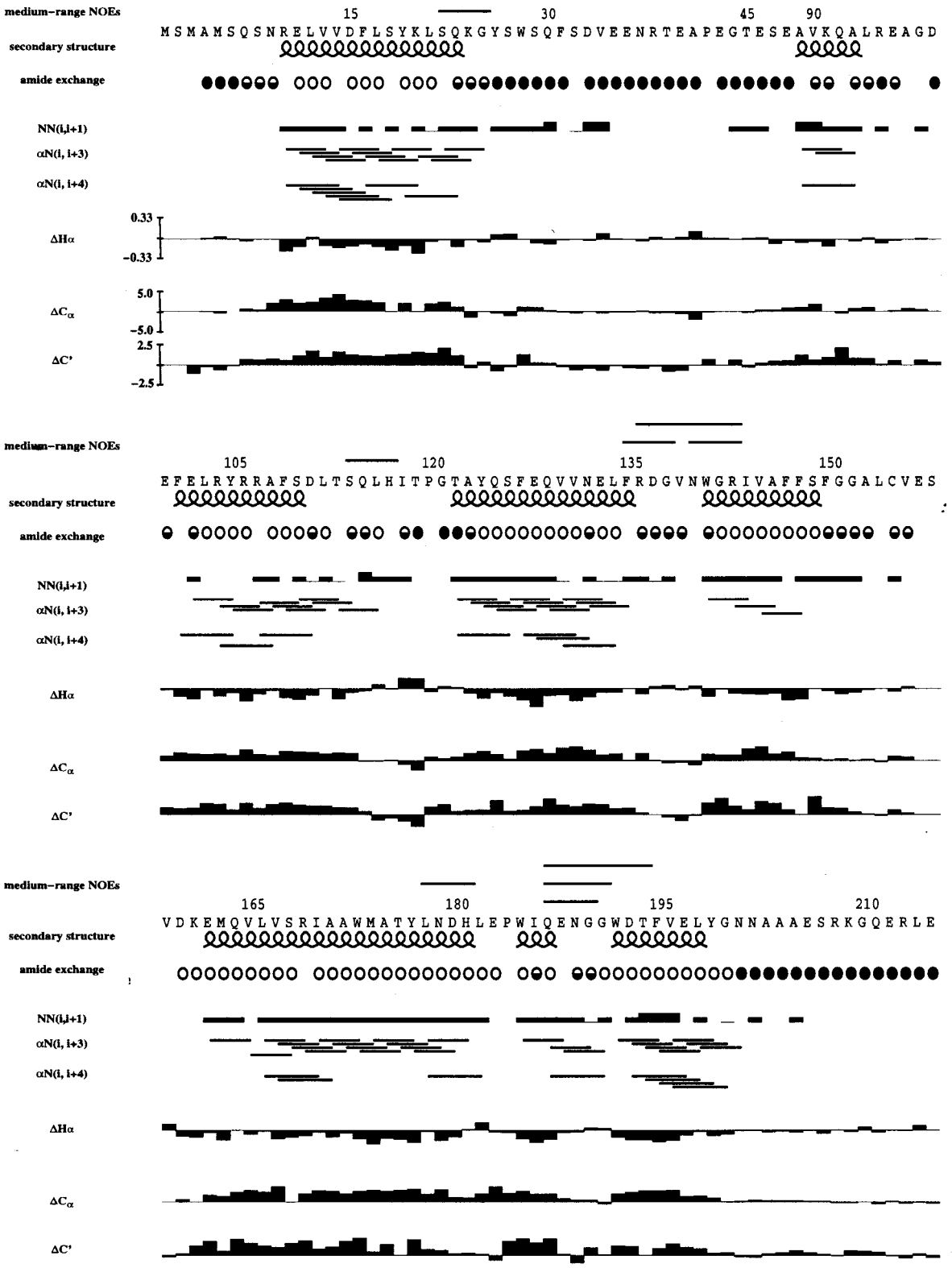

FIGURE 3: Summary of the sequential and medium-range NOEs, amide exchange data, and deviations from random coil chemical shift for H_α, C_α, and C′ for Bcl-x_L in the DPC micelle-bound form. The predicted secondary structure is based on the sequential NOEs and chemicals shifts. The lines above the sequence indicate the observed medium-range NOEs. For the amide exchange data, the open circles indicate no cross-peak to water, while the dark circles indicate a strong NOE cross-peak to water at a mixing time of 100 ms.

Leu182(H_δ), Ile186(H_δ,H_γ)−Gly191(H_α), Ile186(H_δ,H_γ)−Trp192(H_α,H_ϵ,H_ζ), and Ile186(H_α,H_γ,H_δ)−Thr195(H_α,H_ϵ,H_ζ) (Figure 3). These NOEs suggest the presence of tight turns between helix 3/helix 4, helix 4/helix 5, and helix 6/helix 7. The existence of these turns is supported by the $^3J_{N\alpha}$ values for residues in the loops between helix 3/helix 4 and helix 4/helix 5 (*55*). A turn between helices 5 and 6 could not be determined unambiguously because of several missing assignments and resonance overlap. The very limited resolution of the ^{13}C side chain resonances made it difficult to identify any further unambiguous long-range NOE contacts for the protein.

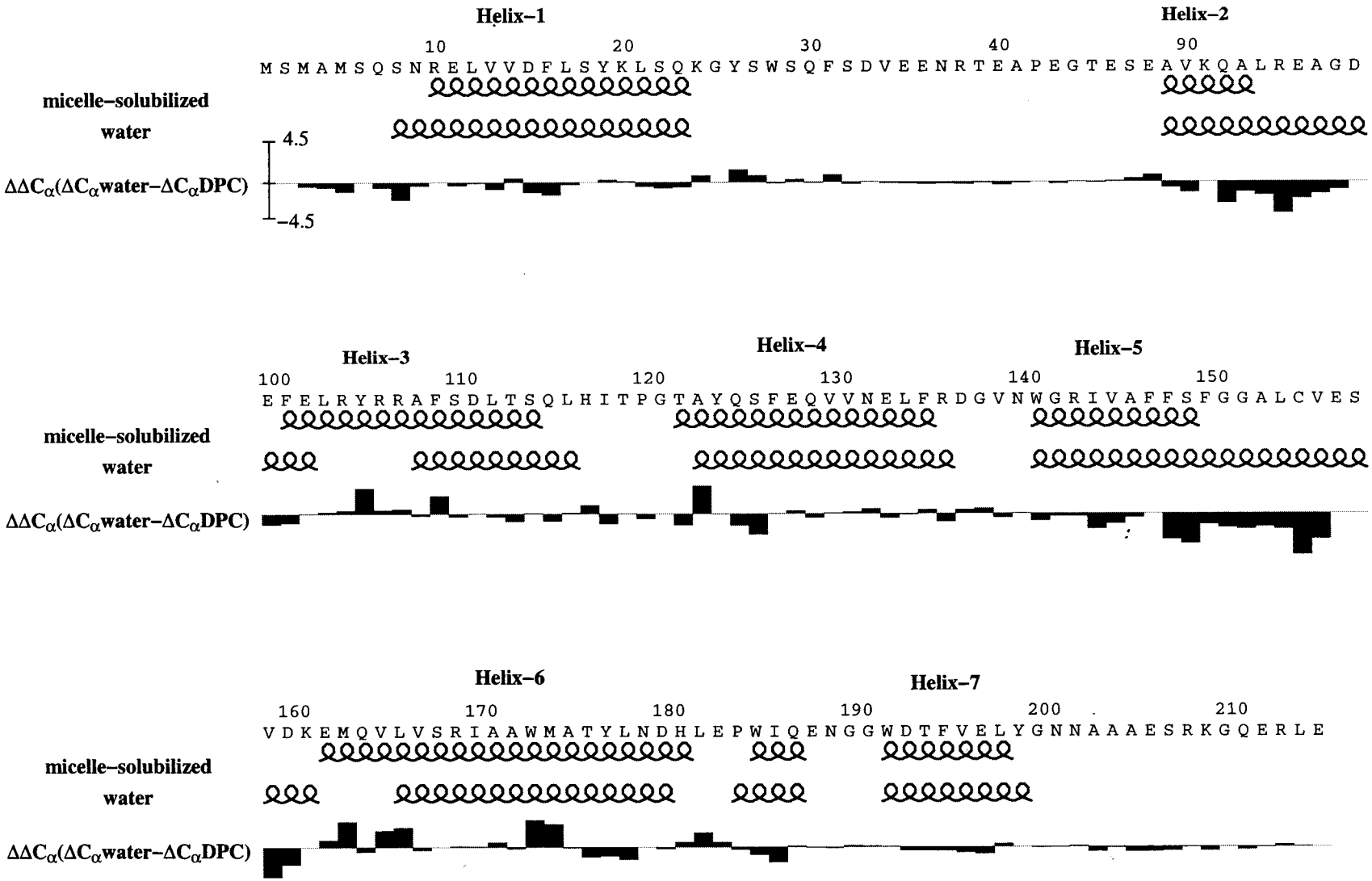

FIGURE 4: Comparison of the secondary structure of Bcl-x_L in the DPC micelle-bound and in the detergent-free form. For reference, the difference between the C_α chemical shift of the two forms is also shown, which clearly indicates the major differences in helix 2 and helix 5.

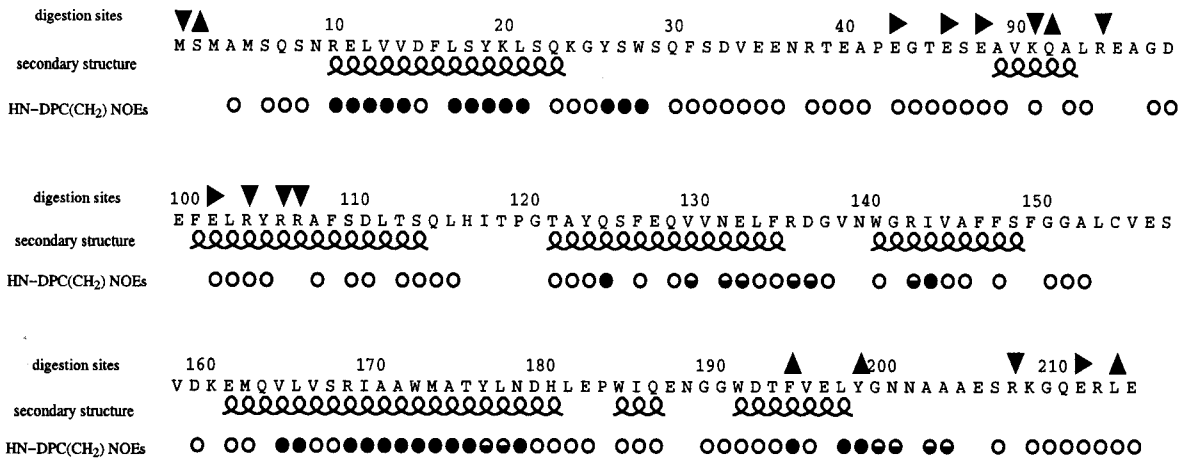

FIGURE 5: Summary of the NOE data describing the protein−detergent contacts and the results of limited proteolysis. HN - DPC(CH_2) refers to the NOE cross-peaks observed between the alkyl chain of DCP (1.23 ppm) and the amide protons of Bcl-x_L. A dark circle indicates a strong NOE cross-peak, a half shaded circle indicates a weak NOE cross-peak, and an open circle indicates no observable NOE cross-peak. No circle indicates that the amide signal was not resolved in the 3D experiment. The observed cut sites by different enzymes are indicated by arrows. Down arrow: trypsin; up arrow: chymotrypsin; and right arrow: endoproteinase Glu-C.

Structural Comparison to Bcl-x_L in Water. Although Bcl-x_L contains several α-helices when free in solution and when incorporated into micelles, there are several distinct differences in the location and length of the helices for Bcl-x_L in the two environments (Figure 4). The most striking differences are for helix 2 and helix 5. These two helices are much shorter in the micelle form of Bcl-x_L. In contrast, helix 6 is much longer for Bcl-x_L when dissolved in detergent micelles. On the basis of the chemical shift information alone, the program TALOS predicts that helix 6 extends all the way to Gln187 in micelles. However, the lack of the characteristic short-range and sequential NOEs near Pro184 suggests a break or kink in this helix.

Several long-range NOEs that are observed in the aqueous form of Bcl-x_L are not observed in the micelle-solubilized form. For example, the Ile144 methyl group in water has NOEs to Leu 94, Leu182, and Ile186, indicative of the close packing of three different α-helices. However, none of these NOEs are present in the DPC micelle-bound form of Bcl-x_L. This clearly shows that the tertiary fold of the micelle-bound Bcl-x_L is different from that of the form in water. The low chemical shift dispersion and the lack of any upfield shifted methyl resonances for micelle-bound Bcl-x_L are consistent with this conclusion. In the detergent-free protein, upfield shifted methyls are observed as a consequence of the methyls packing against aromatic residues in the hydrophobic core of the protein. The lack of upfield shifted methyl resonances in the detergent-solubilized form of Bcl-x_L suggests that the protein−protein contacts in native Bcl-x_L are replaced in the micelle environment by interactions with the detergent.

Limited Proteolysis. Limited digestion experiments were performed using three different enzymes: trypsin, chymotrypsin, and endoproteinase Glu-C. These enzymes were chosen to allow the testing of both hydrophobic (F, Y, W, and L) and hydrophilic (K, R, and E) sites for protease accessibility. The pattern and time for the digestion were compared for the protein in water and in micelles. The protein in water was highly resistant to digestion. After initial cuts in the C- and N-terminal regions, the core of the protein was stable for over 4 h. In micelles, the protein was digested more rapidly, but several stable fragments were protected for over an hour. The sites of digestion in the two environments were also different. There are a large number of possible digestion sites in the protein, but only a few of them are cut during the first hour of digestion in DPC micelles. These sites are localized to residues 40−110 and to the C-terminus (Figure 5). The cuts at Arg104, Arg106, and Arg107 were minor as compared to the other sites. Interestingly, an unusual chymotrypsin digestion site was observed C-terminal to Gln52.

Although both the NOE and the amide exchange data indicate the presence of a long, flexible loop between residues 25−89, digestion only occurs between residues 40−110. Furthermore, some of the cut sites are in regions with secondary structure elements, indicating that helix 2 and helix 3 are very dynamic and that the loop region between residues 26−40 is more protected from digestion than these helices. This protection is most likely due to contact with the DPC micelles (see below).

Characterization of Protein-Detergent Interactions. Further insight into the behavior of Bcl-x_L in the micelle environment can be gained from NOEs between the protein and the detergent. These NOEs were obtained by using a 200-ms ^{15}N-resolved NOESY experiment on 100% perdeuterated protein in protonated DPC. Figure 6 shows strip plots extracted from this 3D experiment for several residues from different sections of the protein. Some parts of the protein have no direct contact with the micelles as evident by the lack of NOEs to detergent and by the fast amide exchange rates. These regions are the C- and N-termini, the second part of the long loop (residues >30), helix 2, and helix 3. Helix 4 and helix 7 show several weak detergent−amide NOEs, suggesting that these helices are in contact with the micelle. On the basis of our data, it is not possible to characterize this association, although it is probable that these helices associate mainly with the headgroup region of the micelle. Helix 1 and helix 6 show several strong NOEs to the detergent, suggesting that these helices are at least partially embedded in the hydrophobic core of the micelle. Similarly, the initial segment of the long loop

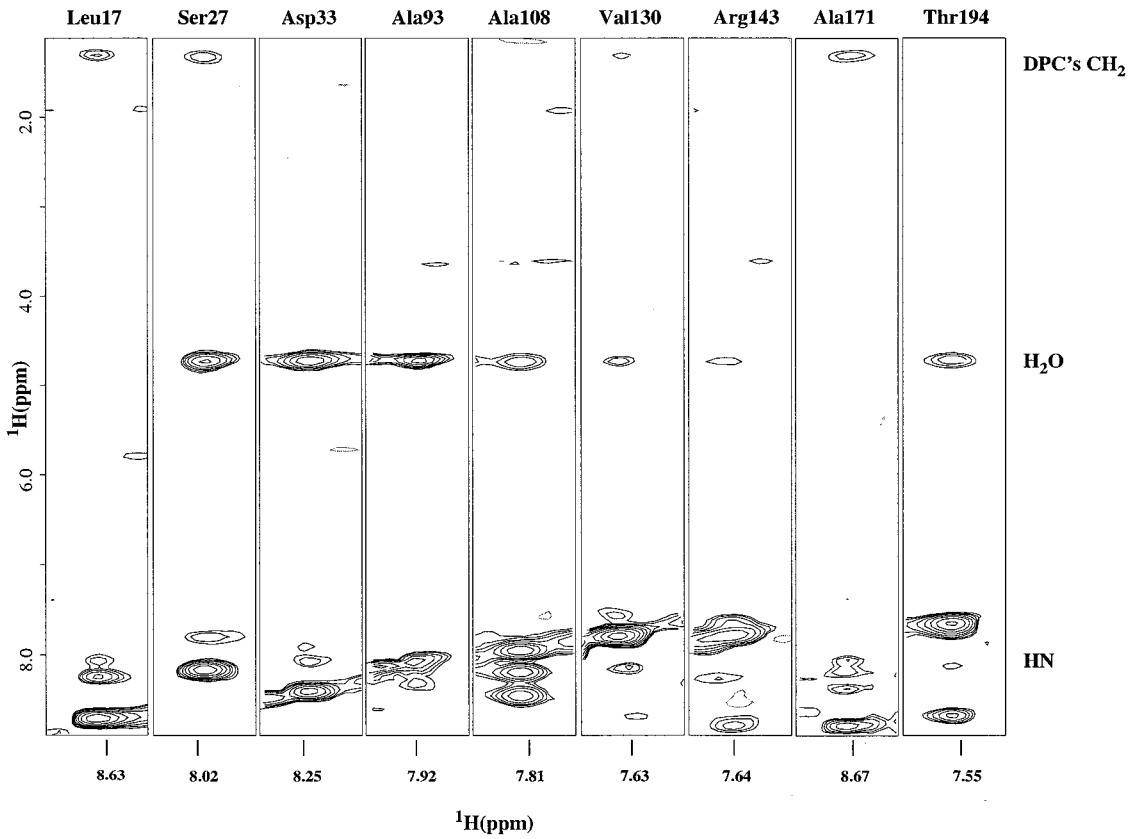

FIGURE 6: Representative slices from the ^{15}N-resolved NOESY experiment (τ = 200 ms) of 100% deuterated Bcl-x_L in protonated DPC micelles.

(residues 26−30) show strong NOEs to the detergent chain and protection from digestion. It seems likely that this part of the loop, which does not have any regular secondary structure, is also embedded in the hydrophobic part of the micelle. Helix 5 is the most hydrophobic of all the α-helices of Bcl-x_L, but its interaction with the micelle could not be well-characterized in this study because of severe resonance overlap. The data for the short loop connecting helix 5 and 6 show no NOEs to the DPC chain, indicating very limited interaction with the micelle.

These results support that helix 1, and possibly helix 5, protrude into the micelle and contact its hydrophobic interior without fully spanning its length. This is very similar to the positioning of the α-helices of the KcsA K^+ channel's selectivity filter (*57*). Of the seven helices identified in Bcl-x_L, helix 6 is long enough to span a bilayer, and it shows an interaction with the micelle interior. However, this helix contains a charged Arg and an Asp residue. To exist in the hydrophobic core of the micelle, such charged residues need to be accommodated by either being exposed to solvent or by the formation of salt bridges. The role of strongly hydrogen bonding groups in membrane protein folding is suggested to play an important role (*58*, *59*), but no evidence was found to support the existence of these in the micelle solubilized form of Bcl-x_L. Another possibility is that helix 6 is only partially embedded in the micelle with its charged side chains extending toward the region of the detergent's headgroup.

Mobility of Bcl-x_L in Micelles. The internal mobility of Bcl-x_L in micelles was characterized by measuring the steady-state [^{1}H,^{15}N]-NOEs and T_1 and T_2 relaxation times. The shortest T_2 and longest T_1 values were observed for helices 1 and 6, suggesting that the mobility of these Bcl-x_L segments are the lowest and are mainly determined by the tumbling of the DPC micelles. T_1 values of 1.1 s and T_2 values of 30 ms were observed for residues in these regions. Assuming isotropic tumbling for these segments of Bcl-x_L, T_1/T_2 ratios indicate a correlation time of close to 30 ns (*60*). This value is in good agreement with expected correlation times for proteins in detergent micelles (*54*) and is longer than the value expected for a 20-kDa protein in aqueous solution (∼10 ns). In addition, the data agree with the observed detergent−protein NOEs and the digestion results, which suggest that helices 1 and 6 are closely associated with the detergent micelle.

For helices 2, 3, 4, 5, and 7, the T_1 values decrease to 0.95 s, and the T_2 values increase on average to 35 ms. Thus, these helices still tumble together with the micelle. In the loops, an even further decrease in the T_1 values (∼0.9 s) and an increase in the T_2 values (40−60 ms) values were observed. In the long flexible loop and the C-terminus of Bcl-x_L in micelles, short T_1 (∼0.7 s) and long T_2 (50−250 ms) values were measured, indicating that these regions are highly mobile relative to the overall tumbling of the micelle.

Negative steady-state NOE values were observed for residues 30−48 in the long loop between helices 1 and 2 and for the C-terminus. The measured values for these segments vary between 0 and −0.4 and are small in absolute value as compared to steady-state NOEs observed in the termini or in the wild-type loop of Bcl-x_L in aqueous solution (*3*). This suggests that while these regions are more mobile relative to the overall tumbling rate of Bcl-X_L in the micelle,

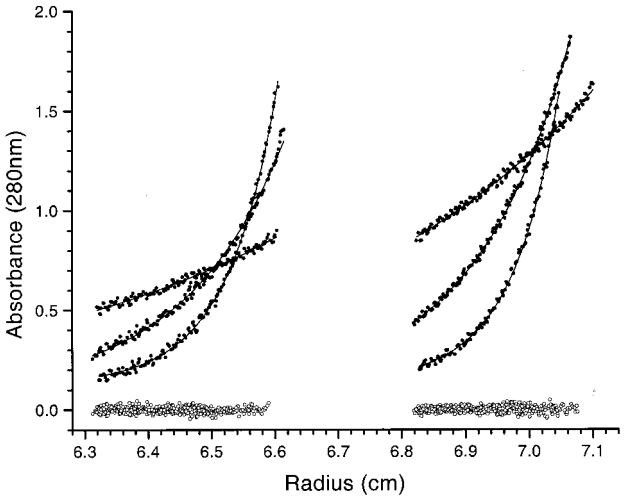

FIGURE 7: Sedimentation equilibrium of Bcl-x_L in DPC micelles. Closed circles are the absorbance data points, the lines indicate the fitted data, and the open circles are the residuals. Initial concentrations of Bcl-x_L were 0.25 and 0.51 mg/mL. The concentration of DPC in this experiment was 50 mM.

they still tumble relatively slowly as compared to similar regions in the free protein.

Oligomerization State. Analytical ultracentrifugation was used to examine the oligomerization state of Bcl-x_L in DPC micelles. When the molecular weight is held as a global parameter and when the two highest concentrations of protein (0.25 and 0.51 mg/mL) were included at three rotor speeds, the data indicate a single ideal species in solution. Data with either buffer (Figure 7) or buffer plus DPC (data not shown) blanks gave molecular weights of 19 200 ± 120 and 19 800 ± 65, respectively. The molecular weight calculated for the sequence is 20 500. These results indicate that this form of Bcl-x_L is a monomer in solution in the presence of DPC micelles, even though DPC micelles are capable of supporting membrane protein oligomerization (*14*, *18*).

CONCLUSIONS

In this study, the behavior of the anti-apoptotic protein Bcl-x_L in a membrane mimetic environment is described. Upon interaction with micelles, Bcl-x_L undergoes a major conformational change that is not triggered by the presence of monomeric detergent. Using multidimensional NMR techniques on perdeuterated Bcl-x_L in DPC-d_{38} micelles, the backbone of the protein was assigned, and the detailed secondary structure of the micelle-bound form of Bcl-x_L was determined. Both in the free and in the micelle-bound form, Bcl-x_L contains seven α-helices. However, a comparison of the secondary structure in the detergent-free and in the detergent-solubilized form of Bcl-x_L revealed several differences in the length and location of these α-helices. Another difference observed for Bcl-x_L in micelles as compared to the protein in aqueous solution is the radical decrease in the chemical shift dispersion of the side chain resonances and the disappearance of the upfield shifted methyl resonances. This suggests that when Bcl-x_L interacts with micelles, protein−protein contacts are replaced with protein−detergent interactions.

On the basis of the relaxation data and the fast amide exchange rates, Bcl-x_L in micelles is dynamic and much less tightly packed than in water. Several medium-range NOEs were assigned in micelle-bound Bcl-x_L indicative of the presence of helix−turn−helix motifs. However, no long-range NOEs were observed. The absence of long-range NOEs for the micelle-bound form of Bcl-x_L indicates that Bcl-x_L in micelles does not adopt the same fold as Bcl-x_L in water.

To further characterize Bcl-x_L in micelles, the protein−detergent interfaces were mapped from limited proteolyic digestion and detergent−protein NOEs. The results from these experiments suggest that helix 1, helix 6, and the initial part of the long loop after helix 1 are embedded in the hydrophobic core of the micelle, while the other helices only interact with the surface of the micelle or make no contact with the detergent.

The major objective for studying Bcl-x_L in a lipid environment was to better understand its structure and function. Bcl-x_L and other Bcl-2 related proteins are localized to the outer membrane of the mitochondria and the outer nuclear and endoplasmic reticulum membranes. Several of these Bcl-2 family proteins form pores in synthetic membranes that might be relevant for their biological activity. On the basis of the estimated size of these channels, it has been hypothesized that Bcl-x_L exists as an oligomer in membranes (*5*). Our ultracentrifugation results, on the other hand, indicate that Bcl-x_L in DPC micelles is in a monomeric state. Thus, in micelles, Bcl-x_L may not be forming a pore. However, recently the relevance of the channel-forming activity of Bcl-2 and Bcl-x_L for their apoptotic function has been questioned. The Bcl-2 family of proteins was shown to regulate cytochrome *c* release and the mithocondrial membrane potential through a direct interaction with the voltage-dependent anion channel (VDAC) (*61*). The region of Bcl-x_L that is responsible for inhibiting VDAC activity is contained within the first α-helix (BH4-domain) (*62*). As shown here, helix 1 is located in the micelle and may also be localized within the mitochondrial membrane where it can interact with VDAC and inhibit its activity. In any case, the conformational features of Bcl-x_L in micelles described here provides useful information on Bcl-x_L in a lipid environment, which may help to explain some of its interesting biological activities.

ACKNOWLEDGMENT

We thank Dr. Eric Hebert for help with the CD studies, Dr. Robert Meadows for assistance with the TALOS program, and Dr. Liping Yu and Dr. Craig Thompson for helpful discussions.

REFERENCES

1. Chao, D. T., and Korsmeyer, S. J. (1998) *Annu. Rev. Immunol. 16*, 395−419.
2. Tsujimoto, Y., and Shimizu, S. (2000) *FEBS Lett. 466*, 6−10.
3. Muchmore, S. W., Sattler, M., Liang, H., Meadows, R. P., Harlan, J. E., Yoon, H. S., Nettesheim, D., Chang, B. S., Thompson, C. B., Wong, S. L., Ng, S. L., and Fesik, S. W. (1996) *Nature 381*, 335−341.
4. Sattler, M., Liang, H., Nettesheim, D., Meadows, R. P., Harlan, J. E., Eberstadt, M., Yoon, H. S., Shuker, S. B., Chang, B. S., Minn, A. J., Thompson, C. B., and Fesik, S. W. (1997) *Science 275*, 983−986.
5. Minn, A. J., Velez, P., Schendel, S. L., Liang, H., Muchmore, S. W., Fesik, S. W., Fill, M., and Thompson, C. B. (1997) *Nature 385*, 353−357.

6. Schendel, S. L., Xie, Z., Montal, M. O., Matsuyama, S., Montal, M., and Reed, J. C. (1997) *Proc. Natl. Acad. Sci. U.S.A. 94*, 5113−5118.
7. Schlesinger, P. H., Gross, A., Yin, X. M., Yamamoto, K., Saito, M., Waksman, G., and Korsmeyer, S. J. (1997) *Proc. Natl. Acad. Sci. U.S.A. 94*, 11357−11362.
8. Antonsson, B., Conti, F., Ciavatta, A., Montessuit, S., Lewis, S., Martinou, I., Bernasconi, L., Bernard, A., Mermod, J. J., Mazzei, G., Maundrell, K., Gambale, F., Sadoul, R., and Martinou, J. C. (1997) *Science 277*, 370−372.
9. Schendel, S. L., Azimov, R., Pawlowski, K., Godzik, A., Kagan, B. L., and Reed, J. C. (1999) *J. Biol. Chem. 274*, 21932−21936.
10. Schendel, S. L., Montal, M., and Reed, J. C. (1998) *Cell Death Differ. 5*, 372−380.
11. Vander Heiden, M. G., and Thompson, C. B. (1999) *Nat. Cell. Biol. 1*, E209−E216.
12. Henry, G. D., and Sykes, B. D. (1992) *Biochemistry 31*, 5284−5297.
13. Williams, K. A., Farrow, N. A., Deber, C. M., and Kay, L. E. (1996) *Biochemistry 35*, 5145−5157.
14. MacKenzie, K. R., Prestegard, J. H., and Engelman, D. M. (1997) *Science 276*, 131−133.
15. Matthey, U., Kaim, G., Braun, D., Wuthrich, K., and Dimroth, P. (1999) *Eur. J. Biochem. 261*, 459−467.
16. Tanford, C., and Reynolds, J. A. (1976) *Biochim. Biophys. Acta 457*, 133−170.
17. Fleming, K. G., Ackerman, A. L., and Engleman, D. M. (1997) *J. Mol. Biol. 272*, 266−275.
18. Kochendoerfer, G. G., Salom, D., Lear, J. D., Wilk-Orescan, R., Kent, S. B., and DeGrado, W. F. (1999) *Biochemistry 38*, 11905−11913.
19. Holzman, T. F., and Snyder, S. W. (1994) in *Modern Analytical Ultracentrifugation*, Birkhauser, Boston, MA.
20. Cohn, E. J., and Edsall, J. T. (1943) in *Proteins, Amino Acids, and Peptides as Ions and Dipolar Ions*, Rheinhold, New York.
21. Bodenhausen, G., and Ruben, D. (1980) *Chem. Phys. Lett. 69*, 185−188.
22. Vuister, G. W., and Bax, A. (1992) *J. Magn. Reson. 98*, 429−435.
23. Kay, L. E., Ikura, M., Tschudin, R., and Bax, A. (1990) *J. Magn. Reson. 89*, 496−514.
24. Matsuo, H., Li, H., and Wagner, G. (1996) *J. Magn. Reson. B 110*, 112−115.
25. Yamazaki, T., Lee, W., Revington, M., Mattellio, D. L., Dahlquist, F. W., Arrowsmith, C. H., and Kay, L. E. (1994) *J. Am. Chem. Soc. 116*, 6464−6465.
26. Yamazaki, T., Lee, W., Arrowsmith, C. H., Muhandiram, D. R., and Kay, L. E. (1994) *J. Am. Chem. Soc. 116*, 11655−11666.
27. Yamazaki, T., Tochio, H., Furui, J., Aimoto, S., and Kyogolu, Y. (1997) *J. Am. Chem. Soc. 119*, 872−880.
28. Bax, A., Clore, G. M., and Gronenborn, A. M. (1990) *J. Magn. Reson. 88*, 425−431.
29. Logan, T. M., Olejniczak, R., Xu, R. X., and Fesik, S. W. (1993) *J. Biomol. NMR 3*, 225−231.
30. Marion, D., Kay, L. E., Sparks, S. W., Torchia, D. A., and Bax, A. (1989) *J. Am. Chem. Soc. 111*, 1515−1517.
31. Fesik, S. W., and Zuiderweg, E. R. P. (1988) *J. Magn. Reson. 78*, 588−593.
32. Ikura, M., Kay, L. E., Tschudin, R., and Bax, A. (1990) *J. Magn. Reson. 86*, 204−209.
33. Kuboniwa, H., Grzesiek, S., Delaglio, F., and Bax, A. (1994) *J. Biomol. NMR 4*, 871−878.
34. Kay, L. E., Keifer, P., and Saarinen, T. (1992) *J. Am. Chem. Soc. 114*, 10663−10665.
35. Tolman, J. R., Chung, J., and Prestegard, J. H. (1992) *J. Magn. Reson. 98*, 660−664.
36. Muhandiram, D. R., and Kay, L. E. (1994) *J. Magn. Reson. B 103*, 203−216.
37. Palmer, A. G. I., Cavanagh, J., Wright, P. E., and Rance, M. (1991) *J. Magn. Reson. 93*, 151−170.
38. Grezesiek, S., and Bax, A. (1993) *J. Am. Chem. Soc. 115*, 12593−12594.
39. Shaka, A. J., Keeler, T., Frenkiel, T., and Freeman, R. (1983) *J. Magn. Reson. 52*, 335−338.
40. Shaka, A. J., Barker, P. B., and Freeman, R. (1985) *J. Magn. Reson. 64*, 547−552.
41. Emsly, L., and Bodenhausen, G. (1990) *Cheme. Phys. Lett. 165*, 469−476.
42. Shaka, A. J., Lee, C. J., and Pines, A. (1988) *J. Magn. Reson. 52*, 335−338.
43. Olejniczak, E. T., and Eaton, H. L. (1990) *J. Magn. Reson. 87*, 628−632.
44. Farrow, N. A., Zhang, O., Forman-Kay, J. D., and Kay, L. E. (1994) *J. Biomol. NMR 4*, 727−734.
45. Wang, J., Sahoo, D., Sykes, B. D., and Ryan, R. O. (1998) *Biochem. Cell Biol. 76*, 276−283.
46. Chen, Y., Yang, J. T., and Chau, K. H. (1974) *Biochemistry 13*, 3350−3359.
47. Gardner, K. H., and Kay, L. E. (1998) *Annu. Rev. Biophys. Biomol. Struct. 27*, 357−406.
48. Cavanagh, J., Fairbrother, W. J., Palmer, A. G., and Skelton, N. J. (1996) in *Protein NMR Spectroscopy. Principles and Practice*, Academic Press, Inc., San Diego, CA.
49. Clore, G. M., and Gronenborn, A. M. (1994) *Methods Enzymol. 239*, 349−363.
50. Logan, T. M., Olejniczak, E. T., Xu, R. X., and Fesik, S. W. (1992) *FEBS Lett. 314*, 413−418.
51. Wishart, D. S., Sykes, B. D., and Richards, F. M. (1992) *Biochemistry 31*, 1647−1651.
52. Wishart, D. S., and Sykes, B. D. (1994) *J. Biomol. NMR 4*, 171−180.
53. Cornilescu, G., Delaglio, F., and Bax, A. (1999) *J. Biomol. NMR 13*, 289−302.
54. Henry, G. D., and Sykes, B. D. (1994) *Methods Enzymol. 239*, 515−535.
55. Wuthrich, K. (1986) in *NMR of Proteins and Nucleic Acids*, John Wiley & Sons, Inc., New York.
56. Karplus, M. (1963) *J. Am. Chem. Soc. 85*, 2870−2871.
57. Doyle, D. A., Morais Cabral, J., Pfuetzner, R. A., Kuo, A., Gulbis, J. M., Cohen, S. L., Chait, B. T., and MacKinnon, R. (1998) *Science 280*, 69−77.
58. Xiao Zhou, F., Cocco, M. J., Russ, W. P., Brunger, A. T., and Engelman, D. M. (2000) *Nat. Struct. Biol. 7*, 154−160.
59. Choma, C., Gratkowski, H., Lear, J. D., and DeGrado, W. F. (2000) *Nat. Struct. Biol. 7*, 161−166.
60. Kay, L. E., Torchia, D. A., and Bax, A. (1989) *Biochemistry 28*, 8972−8979.
61. Shimizu, S., Narita, M., and Tsujimoto, Y. (1999) *Nature 399*, 483−487.
62. Shimizu, S., Konishi, A., Kodama, T., and Tsujimoto, Y. (2000) *Proc. Natl. Acad. Sci. U.S.A. 97*, 3100−3105.

BI000919V